Research Square

Preprints are preliminary reports that have not undergone peer review.
They should not be considered conclusive, used to inform clinical practice,
or referenced by the media as validated information.

Analysis of the Impact of Complex Topography on the Accuracy of Deformation Monitoring by Radar Interferometry

Zhonghua Zhao
Northeastern University
SHUHONG Wang
shwangneu@126.com
Northeastern University
Junling Yang
Northeastern University
Ji Qi
Liaoning Technical University

Research Article

Keywords: Open-pit mine, D-InSAR, SBAS-InSAR, Multi-source DEM, Deformation monitoring

Posted Date: November 4th, 2026

DOI: https://doi.org/10.21203/rs.3.rs-10949331/v1

License: This work is licensed under a Creative Commons Attribution 4.0 International License.
Read Full License

Analysis of the Impact of Complex Topography on the Accuracy of Deformation Monitoring by Radar Interferometry

Zhonghua Zhao[1,2,3], Shuhong Wang[1,2*], Junling Yang[1,2,4], Ji Qi[5]

1- School of Resource and Civil Engineering, Northeastern University, Shenyang 110819, China
2- International Joint Laboratory for Smart Underground Engineering Construction and Disaster Resilience Prevention, Northeastern University, Shenyang 110819, China
3- School of Intelligent Construction and Environmental Engineering, Shenyang Urban Construction University, Shenyang 110167, China
4- Shen Kan Engineering & Technology Corporation, MCC, Shenyang 110015, China
5- School of Surveying and Mapping and Geographical Science, Liaoning Technical University, Fuxin 123000, China
* Corresponding authors: shwang@mail.neu.edu.cn

Abstract: Interferometric Synthetic Aperture Radar (InSAR) technology offers significant advantages for large-scale, high-precision deformation monitoring and has become a vital method for tracking surface deformation in open-pit mines. However, in areas with complex topography, such as deep concave open-pit mines, radar side-looking geometric distortions and phase aliasing induced by multi-level benches, high-steep slopes, and rugged terrain make Differential InSAR (D-InSAR) and Time-Series InSAR techniques (e.g., SBAS-InSAR) highly sensitive to Digital Elevation Model (DEM) accuracy. Existing research has predominantly focused on flat or gently sloping terrain, leaving a gap in the systematic understanding of error propagation mechanisms across multi-source DEMs and their quantitative impact on InSAR deformation inversion accuracy under complex stepped terrain conditions. Taking the Henan Nannihu Molybdenum Mine as a case study, this study systematically analyzes and compares how multi-source DEMs (ALOS 12.5m, SRTM 30m/90m, TanDEM-X 90m) influence the accuracy of D-InSAR and SBAS-InSAR deformation monitoring. The results indicate that: 1) D-InSAR is extremely sensitive to DEM vertical accuracy. The high-resolution (12.5m), high-accuracy (absolute vertical accuracy of 4.9m) ALOS DEM and its deformation monitoring results are significantly superior to those from SRTM and TanDEM-X DEMs. Its deformation interpretation error is only 0.03–25 mm, and for every 1-meter increase in DEM elevation error, millimeter-level deformation error can be amplified. Furthermore, in areas with slopes >20%, the phase error from the SRTM DEM can be 3–4 times greater than that of the ALOS DEM. 2) SBAS-InSAR exhibits low sensitivity to DEM errors. By leveraging its multi-temporal phase unwrapping and residual phase correction mechanisms, the differences in monitoring results between various DEMs are restricted to only about 3.9 mm. Systematic elevation errors in DEMs cause significant discrepancies in D-InSAR results, particularly along steep slopes and abrupt terrain transition zones. In contrast, the variations in SBAS-InSAR results across different DEM datasets are relatively minor. This demonstrates that the two InSAR techniques exhibit distinct distinctly different sensitivities to external DEM inaccuracies. Accordingly, the following optimization

strategies are proposed: D-InSAR should prioritize using high-precision ALOS DEM whereas SBAS-InSAR can utilize TanDEM-X DEM combined with Ground Control Points (GCPs) to compensate for errors induced by stepped terrain. Ultimately, this research provides a crucial quantitative theoretical basis and practical guidance for selecting optimal DEM data for InSAR deformation monitoring in complex topographic regions.
Keywords: Open-pit mine; D-InSAR; SBAS-InSAR; Multi-source DEM; Deformation monitoring

Introduction

In recent years, the extraction of energy and mineral resources has contributed tremendously to China's economic development. Among the available extraction methods, open-pit mining has become a primary approach for recovering energy minerals like coal due to its low mining cost and high recovery rates. However, large-scale open-pit mining inevitably triggers geological hazards such as slope instability, land subsidence, and landslides. These events pose serious threats to personnel safety and equipment stability. Therefore, research on deformation monitoring methods for open-pit mines is of vital practical importance(Li et al. 2022). Traditional monitoring methods, such as the Global Positioning System (GPS), can provide accurate deformation information at specific locations. However, the density of these data points is usually low, making full-coverage monitoring impossible to achieve. Furthermore, GPS tracking involves high station setup costs and maintenance difficulties. Conversely, Interferometric Synthetic Aperture Radar (InSAR), an innovative earth observation technology, captures surface deformation by analyzing the phase difference in radar signals, offering a powerful new approach for surface deformation monitoring. This technology can acquire spatially continuous surface deformation data over a short intervals, achieving a monitoring accuracy at the centimeter or even millimeter level(Portela et al. 2024).

Recent open-pit mining studies have shown that satellite InSAR can provide valuable spatial information for slope-performance monitoring, while interpretation remains strongly influenced by changing pit geometry, surface conditions, and the spatial coverage of coherent radar targets (Bar and Dixon 2021). Mining subsidence prediction is conducted by integrating the DInSAR technique with a grid-search optimized support vector regression algorithm (Sui et al. 2020), using the Dafosi Coal Mine in Shaanxi Province as the study area. The prediction results of this method align closely with GPS field measurements, yielding a maximum absolute error under 3.1 cm and a maximum relative error below 14%. Consequently, this approach enables high-accuracy mining subsidence prediction in the Loess Plateau and provides crucial support for early-warning mine disaster system. Recent studies confirm that under ideal topographic conditions(Crosetto et al. 2016), InSAR technology can achieve millimeter-level deformation monitoring accuracy ($\sigma < 3$ mm/yr), with a measurement point density of 100–500 points/km², far exceeding that of traditional GNSS monitoring networks(Gong et al. 2021). External Digital Elevation Models (DEMs) must be introduced during InSAR processing to isolate the topographic phase from the

deformation phase. However, during this process, DEM elevation errors propagate directly into the final deformation interpretation results through geometric projection relationships(Niraj et al. 2023). According to research by Zebker et al., the deformation error Δd caused by a DEM elevation error δ can be expressed as $\Delta d = \lambda R \sin\theta\, \delta/(4\pi B\perp)$, where λ is the wavelength, $B\perp$ is the perpendicular baseline, and θ is the incidence angle(Ansar et al. 2022). While this relationship demonstrates a linear association between DEM error and deformation monitoring accuracy, the model fails to account for the non-linear error amplification effects induced by complex topography. For instance, in stepped slope areas, insufficient DEM resolution prevents the accurate characterization of elevation jumps at bench edges. This limitation(Zink et al. 2014) leads to phase unwrapping path errors and increases the error propagation coefficient by 2 to 3 times. Therefore, in complex terrain areas, the accuracy of the DEM itself is a critical factors affecting InSAR monitoring precision.

Differential InSAR (D-InSAR) is a core branch of InSAR technology. It removes the topographic phase by introducing an external DEM, thereby extracting millimeter-level surface deformation signals. This process first involves generating an interferogram from master and slave images that contain both topographic and deformation information. Then, a reference DEM is used to simulate the topographic phase. Finally, the deformation information is isolated through differential processing(Parwata et al. 2020). Compared to traditional InSAR, D-InSAR offers advantages such as high processing efficiency and lower data requirements, making it particularly suitable for short-period, high-dynamic areas such as seismic fault zones and mining slopes(Wessel et al. 2018) However, in practical applications, D-InSAR is extremely sensitive to DEM accuracy, especially in complex terrain environments like open-pit mines or stepped slopes. When terrain undulates drastically and slopes are steep, DEM errors can be amplified into centimeter-level deformation errors through geometric projection; they can even cause aliasing between deformation phase and the residual topographic phase(Li et al. 2025). In the study of an open-pit mine in Indonesia(Parwata et al. 2020), found that when using the SRTM DEM (90m resolution, ~16m vertical accuracy), errors in the differential results could exceed 15 mm in areas with slopes steeper than 25°.

To overcome the high sensitivity to DEM errors in D-InSAR, the Small Baseline Subset InSAR (SBAS-InSAR) technique emerged. This technique employs joint processing of multiple interferograms to construct a time-series deformation model, effectively averaging out DEM errors and atmospheric phase delays. In the study of surface subsidence in a Sichuan mining area, found that SBAS-InSAR(Zhu et al. 2024) could reduce the time-series deformation fluctuations caused by DEM errors from ±15 mm to ±5 mm, significantly improving the stability of deformation monitoring. However, in open-pit mines with rugged terrain, despite its good capability for time-series deformation monitoring, SBAS-InSAR still faces dual challenges regarding accuracy and stability in benched slope areas. Because multitemporal InSAR requires reliable phase unwrapping across space and time, discontinuities and low-coherence areas can introduce unwrapping errors and systematic offsets; minimum-cost-flow formulations are commonly used to improve this step (Pepe and Lanari 2006). Open-

pit case studies have also demonstrated the value of combining satellite InSAR with ground-based radar for identifying accelerating slope deformation in geometrically complex mine settings (Carlà et al. 2018). Furthermore, in the study of the Dagushan Open-pit Iron Mine in Liaoning, demonstrated that even when using multi-track SBAS-InSAR methods, challenges like discontinuous interferometric phases and propagation of topographic errors persist in high-steep slope areas. In these zones, deformation monitoring is significantly affected by the coupling of rock properties, joints, and precipitation. Therefore, enhancing the applicability of SBAS-InSAR in benched open-pit mines urgently requires the synergistic optimization of high-resolution DEMs and adaptive unwrapping algorithms, alongside strengthened quantitative research on error propagation mechanisms.

Although the global coverage of multi-source DEM data (SRTM, ALOS, TanDEM-X) is continuously expanding, the underlying mechanisms driving their performance differences- and their subsequent impact on InSAR monitoring under complex topographic conditions- still present three major scientific questions that must be resolved: ① How does the spatial heterogeneity of DEM errors induced by stepped topography quantitatively affect the deformation interpretation accuracy of D-InSAR and SBAS-InSAR?(Liu et al. 2020) ② Is there a threshold effect regarding the ability of DEMs with different resolutions (e.g., 12.5m vs. 90m) to accurately characterize micro-topography at bench edges?(Rizzoli et al. 2017)③ Do systematic DEM elevation biases (e.g., the 5-10m difference between SRTM and TanDEM-X) trigger non-linear error propagation in steep slope areas?(Gdulová et al. 2020).

To address these questions, this study focuses on the Nannihu Molybdenum Mine in Henan Province as the primary study area. A dataset consisting of 28 Sentinel-1A SAR images and four DEM datasets (ALOS 12.5 m, SRTM 30 m, SRTM 90 m and TanDEM-X 90 m) was utilized. Using identical SAR data, processing workflows, and key parameters, we performed D-InSAR and SBAS-InSAR deformation inversions. By comparing the resulting deformation fields, typical profiles, and representative points, we analyzed the discrepancies in deformation measurements caused by different DEMs in deep-concave, stepped terrains. Particular emphasis is placed on evaluating the distinct responses of D-InSAR and SBAS-InSAR to external DEM variations, thereby providing a valuable baseline reference (Hawker et al. 2019) for DEM selection and interpretation during InSAR processing in complex open-pit mining areas.

1 Study Area and Research Methods

1.1 Study Area and Data

The study area selected for this research is the Nannihu Molybdenum Mine in Henan Province. As shown in Figure 1, the mining site is located between the Xiong'er Mountains and the Funiu Mountains in the eastern Qinling range. The main ore body lies south of the watershed, situated within a mid-to-high mountain area. Decades of intensive mining have significantly altered most of the original landforms within the mine area. Current mining operations have created multiple benches with steep slope angles ranging from 32° to 64°. Within the open pit, the highest bench elevation stands at +1495 m, while the lowest drops to +1330 m, resulting in a height difference of 165

m. On the northwestern side of the pit, the failure to reserve benches during excavation led to the formation of a 120-meter high, unbenched slope with a 50° angle on the western portion of the northern wall. The eastern side of the mining pit is adjacent to the Sandao Zhuang Molybdenum Mine area. A tailings pond is located on the western side, which has been raised to an elevation of +1392 m, exceeding a height of 50 m. The topography surrounding the mining area is severely incised, featuring well-developed valleys and gullies. Consequently, the local topography of the study area has been excavated into a highly complex, stepped terrain.

To evaluate how different DEMs impact InSAR monitoring accuracy across this complex topographic area-while minimize confounding factors such as temporal and spatial decorrelation caused by long baselines, or atmospheric delays due to climatic humidity—this experiment utilized 28 Sentinel-1A SAR scenes covering a period of nearly one year, from February 2023 to June 2024. Four types of external DEM data covering the study area were selected: ALOS (12.5m), SRTM 1" (30×30m), SRTM 3" (90×90m) (Farr et al. 2007), and TanDEM-X 3" DEM (90×90m) (Grohmann 2018) data. The vertical accuracy of these DEM products is a critical baseline parameter directly governing the subsequent deformation inversion precision. In contrast, the absolute vertical accuracy of the ALOS DEM is approximately 5.0 meters. In contrast, the absolute vertical accuracy of the SRTM DEM varies by region, averaging about 10–16 meters in the mountainous areas of China. Meanwhile, the TanDEM-X DEM, a product specifically engineered for radar interferometry, yields the highest absolute vertical accuracy, reaching approximately 4.0 meters in most regions worldwide. Given that the study area is a bare-rock mining zone with complex terrain, these accuracy metrics establish a critical foundation for analyzing variations in deformation monitoring results across the different DEMs.

1.2 Research Methods

1.2.1 Differential Interferometric Synthetic Aperture Radar (D-InSAR)

The fundamental principle of D-InSAR technology relies on acquiring complex image pairs of the same ground target. This is achieved either through simultaneous observation by a SAR antenna in single-pass mode, or via two nearly parallel observations along repeat orbits. Due to the geometric relationship between the target and the two observation positions, a phase difference is generated, which forms an interferogram. These interferometric fringes contain precise information regarding the difference in slant-range distance from the target point to the two antenna positions(Scott et al. 2017). This difference incorporates noise, the flat-earth effect, atmospheric delay effects, and subtle changes in the Earth's surface occurring between the two imaging instances. By systematically removing these confounding factors during data processing, precise surface deformation information can be derived based on the geometric relationship of the radar antennas, radar parameters, and sensor altitude. The overall processing flow is illustrated in Figure 2. The D-InSAR technical workflow can be systematically divided into six core processing stages. First, focusing is applied to the raw SAR data to generate Single-Look Complex (SLC) image pairs through range and azimuth compression, while simultaneously performing precise estimation of spatial baseline parameters. Subsequently, an interferometric phase model

is constructed by combining a reference Digital Elevation Model (DEM) with a reference ellipsoid model, followed by interferogram generation and flat-earth phase removal. Multi-looking is then applied to the interferogram to obtain intensity data, thereby enhancing the signal-to-noise ratio. A critical subsequent step involves employing adaptive filtering to optimize interferogram quality, and calculating the spatial coherence coefficient to serve as a weight for the subsequent phase unwrapping process (Costantini 1998). During the phase unwrapping stage, the phase ambiguity problem is resolved using the Minimum Cost Flow (MCF) algorithm, and unwrapping anomalies in specific areas are corrected through manual phase editing. Next, orbit refinement is conducted to eliminate residual orbital errors, and a re-flattening process is performed to further remove low-frequency phase components such as atmospheric delays. Finally, based on the phase-to-deformation conversion model, the unwrapped phase is converted into surface displacement quantities. Geocoding (Rosen et al. 2000) is then employed to achieve precise registration between the deformation field and the target geographic coordinate system.

In D-InSAR processing, the two-pass method is one of the most classic and widely adopted techniques. Its core principle lies in utilizing an external DEM to simulate and remove the topographic phase, thereby isolating the deformation phase. When processing data with this method, errors in the external DEM serve as a primary factor limiting monitoring accuracy(Zhu et al. 2021). Specifically, the vertical accuracy of the DEM and the perpendicular baseline length exert a significantl influence on the final results. This topographic phase error contribution can be expressed by Equation (1), where θ is the radar incidence angle, R is the sensor-to-target distance, and λ is the wavelength.

$$\phi = -\frac{4\pi B_{\perp}}{\lambda R \sin\theta}\delta \tag{1}$$

1.2.2 Small Baseline Subset Interferometric Synthetic Aperture Radar (SBAS-InSAR)

The SBAS-InSAR technique(Berardino et al. 2002) can generate large-scale average deformation velocities and long-term time-series deformation results, while simultaneously obtaining Line-of-Sight (LOS) deformation fields with centimeter- to millimeter-level accuracy. The SBAS-InSAR technique operates by selecting appropriate temporal and spatial baseline thresholds (Lanari et al. 2007). Multiple SAR images arranged in chronological order are used to generate interferometric pairs. Based on the connection graph of these pairs, interferogram generation, flattening, filtering, and phase unwrapping are performed sequentially to obtain interferograms. An external DEM and Ground Control Points (GCPs) are introduced to remove and estimate residual phases (Lanari et al. 2004) and to assist the phase unwrapping process(Li et al. 2018). The selection of GCPs in open-pit mining areas should adhere to the following principles: 1) They must not be located on areas of high-frequency residual topographic phase; 2) They must not be located within active deformation zones; 3) They must not be located in areas characterized by abrupt phase changes; 4) They must be positioned in relatively stable, non-deforming areas. The interferograms

then undergo re-flattening and refinement(Li et al. 2019), followed by another round of phase unwrapping using the Minimum Cost Flow method and adaptive filtering. Based on this processing, the time-series surface displacement is calculated. Finally, geocoding is performed to obtain the cumulative surface deformation magnitude and deformation rate within the WGS-84 coordinate system(Minderhoud et al. 2020a). The overall processing flow is illustrated in Figure 3. The SBAS-InSAR processing workflow takes multi-temporal SLC images as its input. First, a connection graph is constructed under the constraints of temporal and spatial baseline thresholds, establishing the network topology of interferometric pairs among the images. High-resolution interferograms are generated by combining a reference DEM with differential interferometry. A three-dimensional phase unwrapping algorithm (3D-Unwrapping) is employed to resolve phase ambiguities caused by the coupling of complex topography and deformation(Hussain et al. 2025). After phase editing to remove low-coherence areas, orbit refinement and GCP-assisted corrections are performed to eliminate systematic orbital errors and residual topographic phases. An initial estimation of the regional average deformation velocity and DEM correction factors is then conducted. Atmospheric delay signals are isolated and separated using atmospheric phase screen modeling. Following iterative optimization, the precise average deformation velocity, DEM residuals, and 3D coordinates (longitude, latitude, height) of Persistent Scatterers (PS) are obtained. Time-series deformation information for specific locations is extracted using spatiotemporal filtering, while an average SAR backscattering intensity map(Bhattacharya et al. 2017) is simultaneously generated to assist target identification.

2 InSAR-Based Deformation Monitoring Results in the Mining Area

2.1 Deformation Monitoring Based on D-InSAR

This study selected two SAR scenes acquired on April 4, 2024, and April 16, 2024. For this image pair, the spatial baseline length was -50.389 m, the temporal baseline was 12 days, and the incidence angle was 33.8°. To systematically investigate the impact of different DEMs on the deformation results, the identical image pair was processed using four different DEM datasets as the sole controlled variable in the two-Pass D-InSAR workflow: ALOS DEM (12.5 m spatial resolution), TanDEM-X 3" DEM (90 m spatial resolution), and SRTM DEM (at both 30 m and 90 m spatial resolutions). All other processing parameters were kept strictly identical. The resulting geocoded deformation maps are presented in Figure 4.

A comparative analysis of the D-InSAR deformation maps indicates that the ALOS 12.5m DEM-leveraging its high resolution and superior vertical accuracy (absolute error of 4.9m)- demonstrates an exceptional capability for characterizing fine details along the stepped slopes (32°–64°) of deep concave open-pit mines. Specifically, it clearly delineates deformation anomaly zones at bench edges, with an error range of only 0.03–25 mm. Conversely, due to insufficient spatial resolution (30–90 m) and larger absolute elevation errors (>10 m), the SRTM 30m/90m DEMs induce spatial smoothing effects within the deformation fields at bench transition zones. This smoothing leads to the attenuation of peak deformation values and a blurring of

boundaries. This issue is particularly pronounced on slopes exceeding >20%, where the phase error of the SRTM DEMs 3 to 4 times greater than that of the ALOS DEM. Furthermore, although the TanDEM-X 90m DEM shares the same resolution as the SRTM 90m DEM, it exhibits superior phase continuity in the northwestern high-steep slope areas (slope >50%). This advantage stems from the inherent adaptability of its radar interferometric data source to bare-rock wall topography (achieving a vertical accuracy of 4.9m). The study further reveals that systematic elevation biases between DEMs-such as the 5.4m discrepancies between the SRTM and TanDEM-X products—can trigger non-linear error propagation in complex terrain environments. This propagation results in D-InSAR monitoring discrepancies of up to 16 mm, thereby confirming that high-precision DEM data are indispensable for reliable deformation monitoring in open-pit mining environments.

2.2 Deformation Monitoring Based on SBAS-InSAR

The experiment utilized 28 Sentinel-1A SAR scenes, which were processed separately using the four DEM datasets: ALOS DEM (spatial resolution 12.5m), TanDEM-X 3" DEM (spatial resolution 90m), and SRTM DEM (spatial resolutions 30m and 90m). The temporal baseline threshold was set to 180 days, the spatial baseline threshold was limited to 5% of the critical baseline, and the range-to-azimuth multi-looking ratio was configured to 4:1. The Minimum Cost Flow method was selected for phase unwrapping, utilizing a coherence threshold of 0.15. Assisted by 25 ground control points, a total of 111 interferograms were generated. The resulting Line-of-Sight deformation time series are presented in Figure 5.

A comparative analysis of the SBAS-InSAR time-series deformation monitoring results indicates that the SBAS-InSAR technique significantly reduces sensitivity to DEM errors. This is achieved primarily through its multi-temporal phase unwrapping and residual phase correction mechanisms, restricting the maximum discrepancy between results obtained from different DEM datasets to merely 3.9 mm. By virtue of its high resolution (12.5 m) and superior vertical accuracy (4.9 m), the ALOS 12.5m DEM preserves the optimal spatial details of the deformation field along the benched slopes (slope angles 32°–64°). Consequently, its deformation interpretation results exhibit the smallest overall discrepancy (0.03–25 mm) when validated against D-InSAR observations. Furthermore, although the insufficient resolution of the SRTM 30m/90m DEMs causes a widening of the deformation transition zones—such as increasing the width of the deformation gradient zone at bench edges from 20 m (with ALOS) to 60 m—SBAS-InSAR's multi-temporal phase optimization effectively suppresses elevation-induced errors (>10 m). Specifically, the large deformation differences observed in D-InSAR (ranging from 6.7–36.2 mm) are mitigated down to just 1.3–6.4 mm in the SBAS workflow. This directly validates the time-series method's capability to statistically minimize random errors. Similarly, the TanDEM-X 90m DEM demonstrates excellent adaptability across bare-rock steep-slope areas (slope >50%). Its systematic elevation bias (such as the 5.4m discrepancy compared to SRTM) is successfully mitigated through time-series phase correction, reducing the deformation rate discrepancy from 16 mm in D-InSAR down to 2.8 mm. This result underscores the non-linear error suppression characteristics of SBAS-InSAR when handling systematic

errors. Ultimately, the study demonstrates that the impact of DEM resolution disparities (12.5 m vs. 90 m) on SBAS-InSAR is predominantly confined to its capability to resolve fine-scale deformation gradients. While the ALOS DEM provides a noticeably clearer characterization of deformation gradients at bench edges, the global deformation trends remain highly consistent (discrepancy < 3.9 mm) across all lower-resolution DEMs.

3 Discussion

3.1 Deformation Analysis of Specified Profiles Based on D-InSAR Results

To quantitatively evaluate the impact of different DEMs on D-InSAR monitoring results and analyze the differences between deformation magnitudes and DEM elevation values along different profiles, five profile lines were extracted across the mining area, as shown in Figure 6. A comparison of these results is presented in Figure 7, where the X-axis represents latitude. The solid lines in four distinct colors represent the D-InSAR deformation monitoring results derived from each of the four DEMs, while the corresponding dashed lines denote their respective elevations. Based on the deformation inversion results and profile analysis, it can be observed that in areas with slopes exceeding than 20%, the deformation results obtained using the ALOS DEM exhibit the smallest discrepancy relative to the SBAS-InSAR time-series results. This indicates its superior relative vertical accuracy, with errors confined to approximately 3 meters. Conversely, the TanDEM-X DEM follows, demonstrating a relative vertical accuracy of about 4 meters. Conversely, the deformation errors from the SRTM DEM are significantly larger, reflecting a poorer relative vertical accuracy exceeding 10 meters. This ranking is consistent with independent multi-DEM evaluations showing that the relative performance of ALOS, SRTM, and TanDEM-X varies with terrain conditions and that steep topography can substantially increase vertical errors (González-Moradas and Viveen 2020).

As clearly observed from Figure 7, in non-mining areas where almost no deformation was detected via InSAR technology (profiles A1A2 and E1E2), the differences in D-InSAR deformation results obtained from different DEMs are relatively minor and tend to be highly consistent. This aligns with the expectations of InSAR error propagation theory, indicating that in areas characterized by weak deformation signals and relatively gentle terrain, the impact of DEM errors on deformation inversion remains limited. Conversely, in mining areas experiencing significant deformation (profiles C1C2, D1D2) as well as those with minor deformation (profile B1B2), the discrepancy in deformation results between the two SRTM DEM resolutions (30m and 90m) is relatively small. This suggests that, at the scale of this study, the resolution disparity between the SRTM DEM products themselves is not the dominant factor driving the variation in deformation results. However, significant differences exist in the D-InSAR deformation results between the TanDEM-X DEM and the SRTM DEM within the deformation zones (particularly profiles B1B2, C1C2, D1D2). This discrepancy primarily stems from differences in their absolute elevation accuracy (especially systematic biases) and the varying capacity of their spatial resolutions to characterize complex, highly undulating terrain.

A notable and distinctive pattern in Figure 7 is the high spatial consistency observed within the deformation zones (profiles B1-B2, C1C2, D1D2) between the discrepancies in elevation values of among the four DEMs and the corresponding variations in their D-InSAR deformation results. For instance, at locations where the DEM elevation differences increase significantly—such as around latitude 33.92° on profile C1–C2—the discrepancies in the D-InSAR deformation results also increase synchronously and markedly. This phenomenon quantitatively and visually confirms that in complex areas like open-pit mines which are characterized by drastic topographic relief and benched features, the vertical accuracy of the DEM (encompassing both random errors and systematic biases) exerts a decisive impact on the accuracy of D-InSAR deformation inversion. Through specific quantitative profile analysis, this study elucidates the direct correlation between the spatial distribution of DEM errors and the spatial distribution of D-InSAR deformation errors more clearly than previous research(Sui et al. 2020; Parwata et al. 2020; Li et al. 2025). The results unequivocally demonstrate that in complex terrain environments such as mining districts, the fidelity of D-InSAR deformation results is highly dependent on DEM accuracy. Consequently, integrating higher-quality DEM data—such as the high-resolution, high-precision ALOS DEM—yields substantially more reliable D-InSAR deformation monitoring results.

3.2 Comparative Analysis of Deformation Results from D-InSAR and SBAS-InSAR

To conduct a comprehensive comparison of the performance of D-InSAR and SBAS-InSAR under varying DEM conditions, 20 random points were selected across the mining area. These verification points were distributed across subsidence zones, uplift zones, and stables areas characterized by negligible deformation. To ensure a robust assessment, the SBAS-InSAR deformation values derived from the four different DEMs for the period from April 4, 2024, to April 16, 2024, were extracted. Given the minimal variances among the four SBAS-InSAR datasets, their mean value was established as the baseline benchmark for comparison against the corresponding D-InSAR monitoring results over the identical timeframe, as detailed in Table 1.

The data in Table 1 clearly demonstrate that regardless of whether points are within zones of uplift, subsidence, or negligible deformation, the differences among the SBAS-InSAR results obtained using the four different DEMs over the identical period are consistently minor, with a mean discrepancy of approximately 3.9 mm. This indicates that the SBAS-InSAR technique- by incorporating an optimization workflow that includes multi-temporal phase unwrapping, residual phase correction (encompassing the estimation of atmospheric and orbital errors), and spatiotemporal filtering(Choopani et al. 2025; Li et al. 2019), -can effectively suppress and average out topographic error propagation typically introduced in single -paired D-InSAR processing. However, this study-conducted in an exceptionally complex, deep concave, stepped terrain environment (with slope anales ranging from 32°–64°)-further constraints this discrepancy to mean level of 3.9 mm, quantitatively validating the strong robustness of SBAS-InSAR against DEM errors in complex topography. This stability holds true even when deploying DEMs with spatial resolutions as low as 90 m,

such as TanDEM-X and SRTM, thereby provides strong empirical justification for utilizing more readily available medium-resolution DEMs (e.g., TanDEM-X) for reliable time-series monitoring in topographically similar regions.

Within the subsidence zones of the mining area (e.g., points 1, 2, 11, 12, 18, 20), comparing the corresponding D-InSAR results reveals that the discrepancies between output generated via the ALOS DEM and the TanDEM-X DEM are relatively minor, with deviations ranging from approximately 0.7 to 16 mm. In contrast, the discrepancies among the D-InSAR monitoring results derived from all four DEMs become significantly more pronounced within the uplift zones (e.g., points 3, 4, 5, 6, 7, 9, 14, 15, 16, and 17).

Specifically, the D-InSAR results derived using the ALOS 12.5m DEM show the smallest discrepancy relative to the SBAS-InSAR mean values (ranging from approximately 0.03 to 25 mm). This minimal variance indicates its capacity to provide single-pair deformation insights closest to the time-series inversion accuracy under complex topographic conditions. Conversely, the discrepancies between the D-InSAR results generated from the two SRTM DEMs (30m/90m) and the SBAS-InSAR benchmark values are significantly larger, expanding to approximately 3 to 31.4 mm. Meanwhile, the variations observed in the D-InSAR results utilizing the TanDEM-X 90m DEM fall intermediate to those of the ALOS and SRTM datasets.

This comparative analysis quantitatively verifies the necessity of utilizing high-resolution, high-accuracy DEM data-such as the ALOS DEM- to secure reliable single-pair D-InSAR deformation results across complex stepped terrain. These insights echo the findings (Parwata et al.2020) in an Indonesian mining district which reported errors exceeding 15 mm when using the SRTM DEM on slopes steeper than 25°. They also align with Sui et al.(2020) regarding how insufficient DEM resolution prompts errors propagation that breaches acceptable phase threshold. The primary novelty of this study lies in explicitly quantifying the absolute accuracy variation (spanning the millimeter to centimeter level) across diverse DEM categories—particularly high-resolution ALOS versus medium-to-low resolution SRTM and TanDEM-X—within D-InSAR workflows. This is accomplished through direct cross-validation against multi-temporally optimized SBAS-InSAR profiles, thereby confirming the pronounced advantage of the ALOS DEM for single-pair observation schemes. Furthermore, the generally superior performance of the TanDEM-X DEM over the SRTM DEM variants in the D-InSAR assessment detailed in Table 1 corroborates its operational advantages across bare-rock, steep slope zones (e.g., northwestern slope exceeding 50%). This performance benefit is fundamentally attributable to its specialized radar data source characteristics and superior vertical accuracy. This is also consistent with open-pit slope studies showing that complex geometry and incomplete radar visibility can complicate the interpretation of deformation patterns, reinforcing the need for careful data-quality control (Carlà et al. 2018). Consequently, these findings suggest that the TanDEM-X DEM serves as a more robust and suitable alternative to the SRTM DEM for D-InSAR processing in topographically analogous regions.

4 Conclusions

(1) The vertical accuracy of the external DEM significantly impacts D-InSAR reliability. within the deep concave open-pit mining district, the D-InSAR results derived from the high-accuracy ALOS 12.5m DEM exhibited smallest discrepancy (0.03–25 mm) relative to the SBAS-InSAR mean values, noticeably outperforming both the SRTM and TanDEM-X products. Empirical assessment confirm that for every 1-meter increase in DEM elevation error, the corresponding D-InSAR deformation error can be amplified to the millimeter level. This amplification is particularly severe across benched terrain zones with slopes exceeding 20%, where the phase errororiginating from the SRTM DEM reached 3 to 4 times that of high-precision alternative. This phenomenon reveals a non-linear amplification mechanism of elevation errors derived by geometric projection effects in steep terrains.

(2) Spatial resolution of Digital Elevation Model (DEM) exerts a significant influence on its capability to characterize bench micro-topography. For stepped open-pit mining areas, the 12.5-m ALOS DEM can distinctly resolve slope discontinuities and local deformation gradients, yielding well-defined deformation zones boundaries along bench edges. In contrast, the 30-m SRTM and 90-m TanDEM-X DEM, owing to their coarse spatial resolutions, exhibit notable smoothing in certain bench transition zones. This smoothing leads to widened deformation gradient zones and attenuated local details. These findings demonstrate that DEM spatial resolution directly impacts the representation of complex stepped terrain and local deformation gradients, with such effects being particularly pronounced on steep high-slopes and bench transition zones.

(3) Systematic elevation bias in DEM exerts a significant impact on D-InSAR deformation results in high-steep terrain. For instance, the bulk elevation difference of approximately 5.4 m between SRTM and TanDEM-X can yield D-InSAR deformation discrepancies of up to 16 mm across slope zones. Spatially, the discrepancies among elevation profiles from different DEM datasets align consistently with the scatter of corresponding D-InSAR deformation outputs. This phenomenon is more prominent on steep slopes and bench transition zones, indicating that complex terrain amplifies the sensitivity of D-InSAR results to local DEM variations. By contrast, the overall discrepancies of SBAS-InSAR results across different DEM inputs are relatively minor, demonstrating that D-InSAR and SBAS-InSAR exhibit distinct sensitivities to external DEM inaacuracies.

(4) Optimization strategies include: ①Prioritizing the use of the ALOS DEM for D-InSAR, combined with local correction using Ground Control Points (GCPs) in areas with slopes >15%; ② Selecting the TanDEM-X DEM for SBAS-InSAR to balance cost and accuracy; ③ Constructing a customized DEM through weighted fusion of ALOS and TanDEM-X to mitigate systematic errors. This framework provides a systematic solution encompassing data selection, error control, and algorithm optimization for open-pit mine slope monitoring, holding significant value for engineering applications.

Acknowledgements

This work was supported by the National Natural Science Foundation of China (Grant Nos. U1602232 and 52374157), the Chinese Government Joint Education Project (D20250052；D20240080), and Key R & D Program of Liaoning Provincial Department of Science and Technology, China (2024021200-JH2/1021)

Conflicts of Interest

There are no conflicts of interest to declare.

Contribution statement

Zhonghua Zhao: Data curation, formal analysis, validation, software, and writing—original draft. Shuhong Wang: Conceptualization, writing—review and editing, and funding acquisition. Junling Yang & Ji Qi: Methodology, supervision, and writing—review and editing.

References

Berardino P, Fornaro G, Lanari R, et al. (2002) A new algorithm for surface deformation monitoring based on small baseline differential SAR interferograms, IEEE Transactions on Geoscience and Remote Sensing. 2002, 40(11): 2375-2383. https://doi.org/10.1109/TGRS.2002.803792

Bhattacharya A, Mukherjee K (2017) Review on InSAR based displacement monitoring of Indian Himalayas: issues, challenges and possible advanced alternatives, Geocarto International. 2017, 32(3):298-321. https://doi.org/10.1080/10106049.2016.1140820

Ansar AMH, Din AHM, Latip ASA, Reba MNM (2022) A short review on Persistent Scatterer Interferometry techniques for surface deformation monitoring. Int Archives Photogrammetry Remote Sens Spat Inform Sci 46:23–31. https://doi.org/10.5194/isprs-archives-XLVI-4-W3-2021-23-2022

Rosen PA, Hensley S, Joughin IR, et al. (2000) Synthetic aperture radar interferometry, Proceedings of the IEEE. 2000, 88(3):333-382. https://doi.org/10.1109/5.838084

Gong C, Lei S, Bian Z, et al. (2021) Using time series InSAR to assess the deformation activity of open-pit mine dump site in severe cold area, Journal of Soils and Sediments. 2021, 21(11):3717-3732. https://doi.org/10.1007/s11368-021-03040-8

Rizzoli P, Martone M, Gonzalez C, et al. (2017) Generation and performance assessment of the global TanDEM-X digital elevation model, ISPRS Journal of Photogrammetry and Remote Sensing. 2017, 132:119-139. https://doi.org/10.1016/j.isprsjprs.2017.08.008

Farr TG, Rosen PA, Caro E, et al. (2007) The Shuttle Radar Topography Mission, Reviews of Geophysics. 2007, 45(2):RG2004. https://doi.org/10.1029/2005RG000183

Hussain S, Pan B, Hussain W, et al. (2025) Integrated PSInSAR and SBAS-InSAR analysis for landslide detection and monitoring, Physics and Chemistry of the Earth, Parts A/B/C. 2025, 139:103956. https://doi.org/10.1016/j.pce.

2025.103956
Lanari R, Mora O, Manunta M, et al. (2004) A small-baseline approach for in vestigating deformations on full-resolution differential SAR interferograms, IEEE Transactions on Geoscience and Remote Sensing. 2004, 42(7):1377-1386. https://doi.org/10.1109/TGRS.2004.828196
Li J, Yang T, Deng W, et al. (2025) Evaluating failure mechanisms of excavation-induced large-scale landslides in Xinjing open-pit coal mine through integrated UAV imagery and 3D simulation, Landslides. 2025, 22(6):2021-2036. https://doi.org/10.1007/s10346-025-02460-8
Li JC, Gao F, Lu JG (2019) An application of InSAR time-series analysis for the assessment of mining-induced structural damage in Panji Mine, China, Natural Hazards. 2019, 97(1):243-258. https://doi.org/10.1007/s11069-019-03639-8
Li X, Huang GW, Zhang Q, Zhao QZ (2018) A new GPS/BDS tropospheric delay resolution approach for monitoring deformation in super high-rise buildings, GPS Solutions. 2018, 22(3):12. https://doi.org/10.1007/s10291-018-0752-8
Li YX, Yang KM, Zhang JH, et al. (2022) Research on time series InSAR monitoring method for multiple types of surface deformation in mining area, Natural Hazards. 2022, 114(3):2479-2508. https://doi.org/10.1007/s11069-022-05476-8
Liu Z, Zhu J, Fu H, et al. (2020) Evaluation of the Vertical Accuracy of Open Global DEMs over Steep Terrain Regions Using ICESat Data: A Case Study over Hunan Province, China, Sensors. 2020, 20(17):4865. https://doi.org/10.3390/s20174865
González-Moradas MDR, Viveen W (2020) Evaluation of ASTER GDEM2, SRTMv3.0, ALOS AW3D30 and TanDEM-X DEMs for the Peruvian Andes against highly accurate GNSS ground control points and geomorphological-hydrological metrics, Remote Sensing of Environment. 2020, 237:111509. https://doi.org/10.1016/j.rse.2019.111509
Minderhoud PSJ, Hlavacova I, Kolomaznik J, Neussner O (2020a) Towards unraveling total subsidence of a mega-delta—The potential of new PS InSAR data for the Mekong delta, Proceedings of the International Association of Hydrological Sciences. 2020, 382:327-332. https://doi.org/10.5194/piahs)382-327-2020
Grohmann CH (2018) Evaluation of TanDEM-X DEMs on selected Brazilian sites: Comparison with SRTM, ASTER GDEM and ALOS AW3D30, Remote Sensing of Environment. 2018, 212:121-133. https://doi.org/10.1016/j.rse.2018.04.043
Crosetto M, Monserrat O, Cuevas-González M, et al. (2016) Persistent Scatterer Interferometry: A review, ISPRS Journal of Photogrammetry and Remote Sensing. 2016, 115:78-89. https://doi.org/10.1016/j.isprsjprs.2015.10.011
Niraj KC, Chatterjee RS, Shukla DP (2023) Estimating the period of probable landslide event using advanced D-InSAR technique for time-series deformat

ion study of Kotrupi region, Geomatics, Natural Hazards and Risk. 2023. https://doi.org/10.1080/19475705.2023.2281245
Parwata INS, Nakashima S, Shimizu N, et al. (2020) Effect of digital elevation models on monitoring slope displacements in open-pit mine by differentia l interferometry synthetic aperture radar, Journal of Rock Mechanics and G eotechnical Engineering. 2020, 12(5):1001-1013. https://doi.org/10.1016/j.jrm ge.2020.01.003
Portela J, Staller A, Béjar-Pizarro M, Hamling IJ (2024) Tectonic deformation i n El Salvador from combined InSAR and GNSS data, Tectonophysics. 202 4, 882:230364. https://doi.org/10.1016/j.tecto.2024.230364
Scott C, Lohman R, Jordan T (2017) InSAR constraints on soil moisture evolu tion after the March 2015 extreme precipitation event in Chile, Scientific Reports. 2017, 7(1):1-9. https://doi.org/10.1038/s41598-017-05123-4
Gdulová K, Marešová J, Moudrý V (2020) Accuracy assessment of the global TanDEM-X digital elevation model in a mountain environment, Remote Se nsing of Environment. 2020, 241:111724. https://doi.org/10.1016/j.rse.2020.1 11724
Sui LC, Ma F, Chen N (2020) Mining subsidence prediction by combining sup port vector machine regression and interferometric synthetic aperture radar data, ISPRS International Journal of Geo-Information. 2020, 9(6):17. https:/ /doi.org/10.3390/ijgi9060390
Wessel B, Huber M, Wohlfart C, et al. (2018) Accuracy assessment of the glo bal TanDEM-X Digital Elevation Model with GPS data, ISPRS Journal of Photogrammetry and Remote Sensing. 2018, 139:171-182. https://doi.org/10. 1016/j.isprsjprs.2018.02.017
Pepe A, Lanari R (2006) On the extension of the Minimum Cost Flow algorit hm for phase unwrapping of multitemporal differential SAR interferograms, IEEE Transactions on Geoscience and Remote Sensing. 2006, 44(9):2374- 2383. https://doi.org/10.1109/TGRS.2006.873207
Lanari R, Casu F, Manzo M, et al. (2007) An overview of the Small BAseline Subset algorithm: A DInSAR technique for surface deformation analysis, Pure and Applied Geophysics. 2007, 164(4):637-661. https://doi.org/10.1007 /s00024-007-0192-9
Carlà T, Farina P, Intrieri E, et al. (2018) Integration of ground-based radar an d satellite InSAR data for the analysis of an unexpected slope failure in a n open-pit mine, Engineering Geology. 2018, 235:39-52. https://doi.org/10.1 016/j.enggeo.2018.01.021
Costantini M (1998) A novel phase unwrapping method based on network prog ramming, IEEE Transactions on Geoscience and Remote Sensing. 1998, 36 (3):813-821. https://doi.org/10.1109/36.673674
Hawker L, Neal J, Bates P (2019) Accuracy assessment of the TanDEM-X 90 Digital Elevation Model for selected floodplain sites, Remote Sensing of E nvironment. 2019, 232:111319. https://doi.org/10.1016/j.rse.2019.111319
Bar N, Dixon R (2021) Unveiling unknowns: Practical application of InSAR fo

r slope performance monitoring and risk management across multiple surface mines, Engineering Geology. 2021, 293:106326. https://doi.org/10.1016/j.enggeo.2021.106326

Zhu M, Yu X, Tan H, et al. (2024) High-precision monitoring and prediction of mining area surface subsidence using SBAS-InSAR and CNN-BiGRU-attention model, Scientific Reports. 2024, 14(1):28968. https://doi.org/10.1038/s41598-024-80446-7

Zhu Y, Qiu H, Yang D, et al. (2021) Pre- and post-failure spatiotemporal evolution of loess landslides: a case study of the Jiangou landslide in Ledu, China, Landslides. 2021, 18(10):3475-3484. https://doi.org/10.1007/s10346-021-01714-5

Zink M, Bachmann M, Brautigam B, et al. (2014) TanDEM-X: The New Global DEM Takes Shape, IEEE Geoscience and Remote Sensing Magazine. 2014, 2(2):8-23. https://doi.org/10.1109/MGRS.2014.2318895

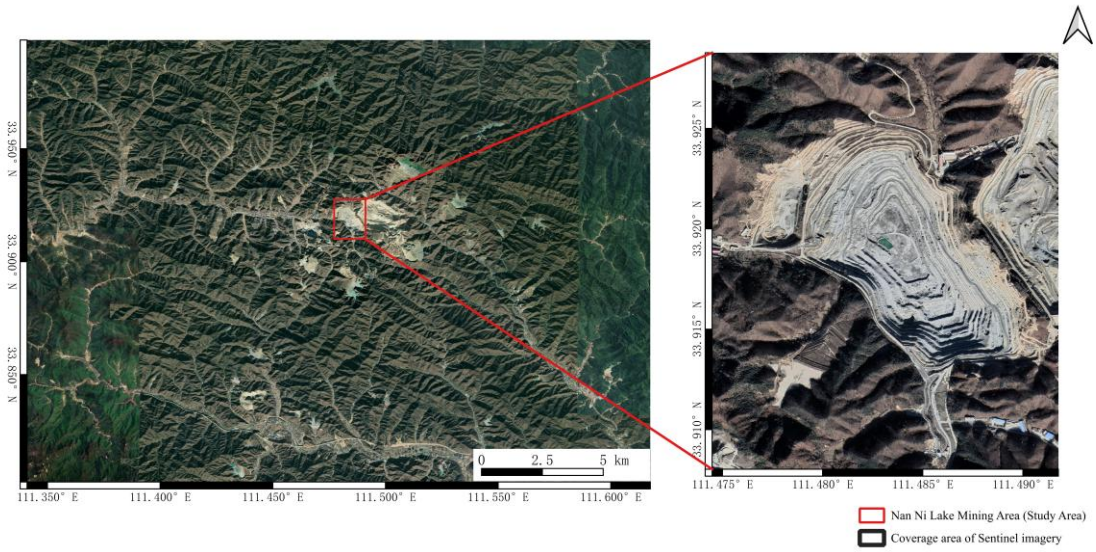
665 Table 1. DInSAR and SBAS InSAR shape variables (unit: mm)

NO.	Latitude	Longitude	ALOS		SRTM 1"		SRTM 3"		TanDEM-X	
			D-InSAR	SBAS-InSAR	D-InSAR	SBAS-InSAR	D-InSAR	SBAS-InSAR	D-InSAR	SBAS-InSAR
1	33°55'8.92"	111°29'17.86"	-8.987	-2.6	-0.766	-10	-3.342	-5.2	-10.245	-3.2
2	33°55'8.69"	111°29'18.48"	-10.978	4.5	-3.038	3.2	-6.528	2.5	-11.736	-1.4
3	33°55'8.61"	111°28'48.18"	16.334	-10	22.388	-2.6	17.895	-7	13.617	-1.8
4	33°55'6.06"	111°28'53.67"	9.5	3.3	16.622	-4	11.921	-3	8.623	3
5	33°55'6.05"	111°28'51.30"	13.687	-0.4	19.26	-6.1	14.222	-0.8	11.875	-2.2
6	33°55'30.02"	111°29'2.51"	15.522	0.9	18.21	0.8	8.366	0.9	17.713	1.1
7	33°55'29.83"	111°29'2.53"	14.775	-0.5	19.881	-0.8	11.351	-0.4	18.047	-1.1
8	33°55'23.18"	111°28'47.76"	3.3	1.5	2.859	6.1	1.568	0.6	19.313	-3
9	33°55'19.22"	111°28'30.72"	20.174	-1.01	11.642	-6.5	25.709	-6.7	14.447	-8.7
10	33°55'19.01"	111°28'47.44"	2.336	0.9	5.605	4.9	14.022	1	16.762	2.7
11	33°55'16.39"	111°29'10.36"	-1.687	-2.3	-3.739	-5.2	-2.672	-3.2	-2.361	-5.1
12	33°55'15.54"	111°29'8.95"	-4.872	-14	-8.321	-16	-10.503	-7.4	-2.861	-11.4
13	33°55'15.06"	111°28'49.50"	4.751	-0.6	10.819	6.6	12.962	-1.3	12.054	2.3
14	33°55'10.63"	111°28'45.11"	15.968	2.6	20.689	5.2	11.998	6.4	17.452	0.9
15	33°54'55.55"	111°29'1.81"	14.445	-9.8	22.506	-4.9	18.427	-6.7	13.534	-3.7
16	33°55'8.45"	111°28'50.12"	13.432	5.2	19.507	1.3	16.262	0	10.173	3.6
17	33°55'8.44"	111°28'45.56"	18.78	0.3	24.711	-2.7	18.407	-9.2	16.568	0.3
18	33°55'16.2"	111°29'9.21"	-3.894	-6.4	-9.52	-6.9	-5.783	-7.1	-2.163	-9.7
19	33°55'15.7"	111°28'48.35"	5.222	1.1	10.864	5	5.306	0.3	14.084	0.6
20	33°55'12.3"	111°29'12.44"	-6.372	-9.4	-2.677	-21	-7.616	-15.3	-3.941	-12.9

666

667

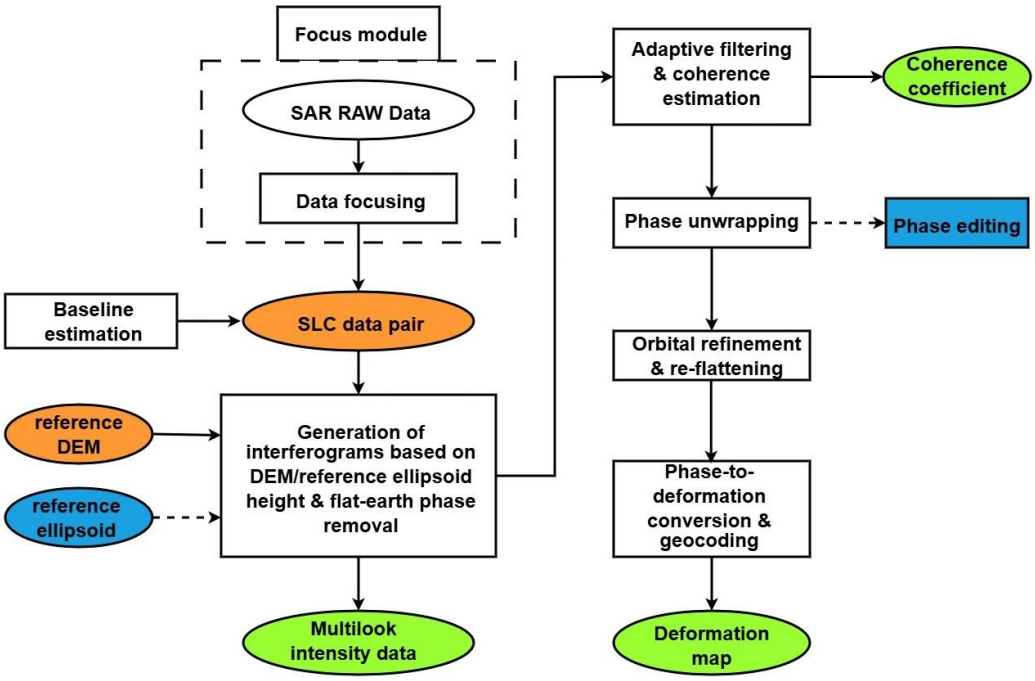
668



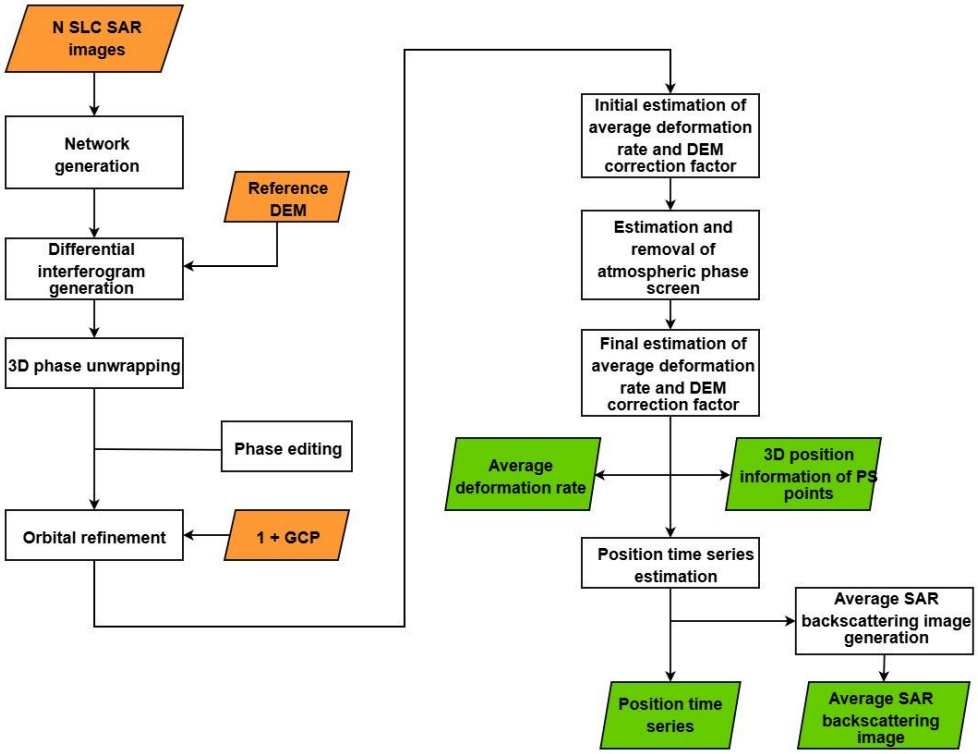
669

670 Fig.1 SAR satellite image coverage area and study area

671



672
673 Fig.2 D-InSAR Data Processing Workflow Diagram
674



675

676 Figure 3. Flow chat of SBAS-InSAR data processing

677

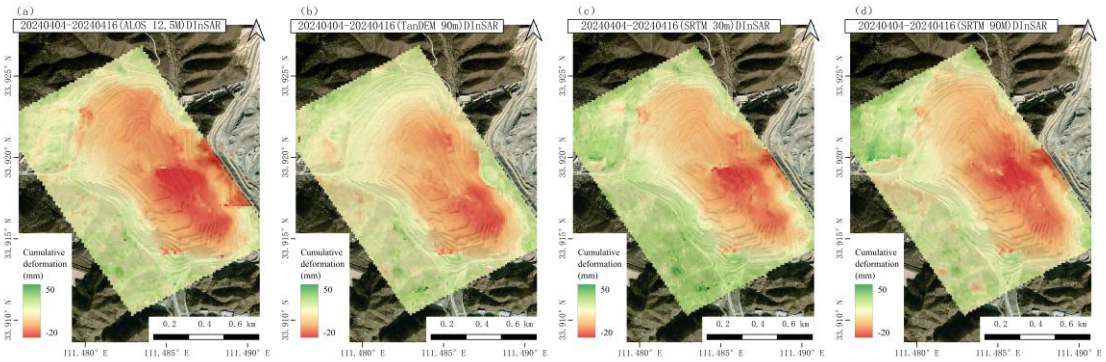


Figure 4. DInSAR deformation(a) Deformation map of external ALOS DEM 12.5 m; (b) Deformation map of external TanDEM-X DEM 90m;(c) Deformation map of external SRTM DEM 30 m; (d)Deformation map of external SRTM DEM 90 m

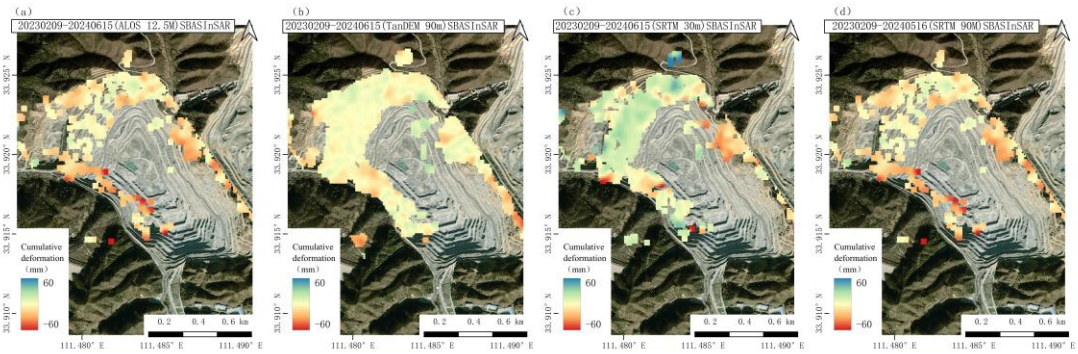


Figure 5. SBAS-InSAR deformation(a) Deformation map of external ALOS DEM 12.5 m; (b) Deformation map of external TanDEM-X DEM 90m ;(c) Deformation map of external SRTM DEM 30 m; (d)Deformation map of external SRTM DEM 90 m

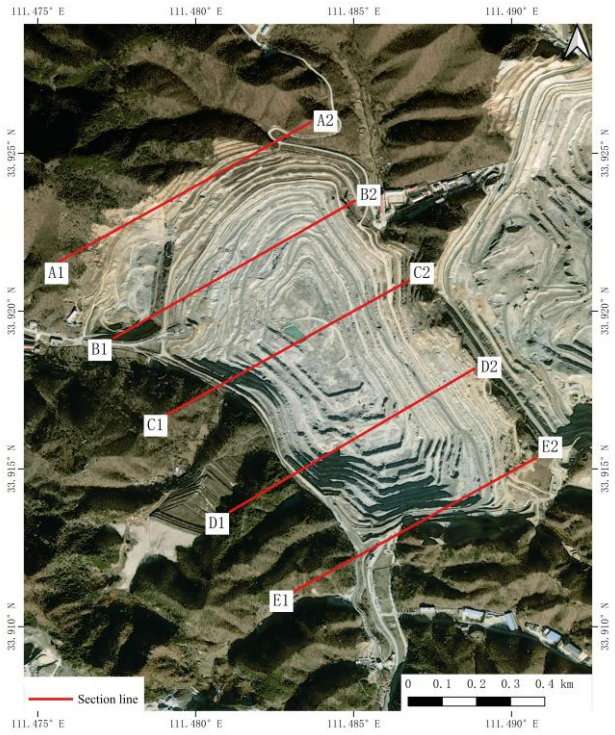
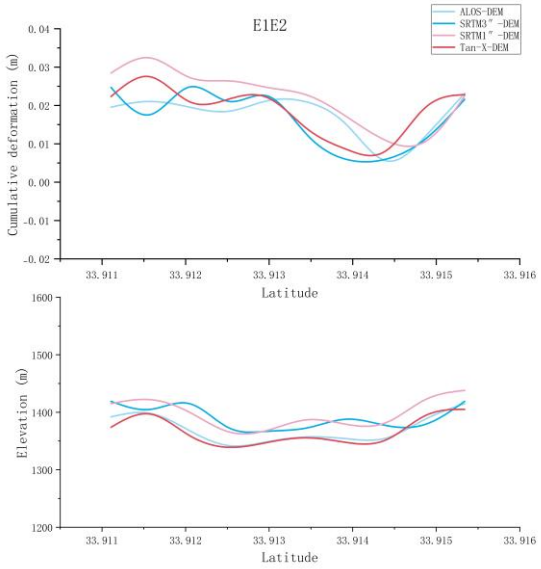


Figure 6. location of section line

691



692
693 Figure 7. Relationship between DInSAR shape variable and latitude
694